SAND2016-2697C

On-Sun Testing of an Advanced Falling Particle Receiver System

Clifford K. Ho,[1, a)] Joshua M. Christian,[1] Julius Yellowhair,[1] Nathan Siegel,[2] Sheldon Jeter,[3] Matthew Golob,[3] Said I. Abdel-Khalik,[3] Clayton Nguyen,[3] and Hany Al-Ansary[4]

[1]*Sandia National Laboratories, P.O. Box 5800, MS-1127, Albuquerque, NM 87185-1127, USA*
[2]*Bucknell University, 1 Dent Drive, Lewisburg, PA 17837, USA*
[3]*Georgia Institute of Technology, 771 Ferst Drive, Atlanta, GA 30332, USA*
[4]*King Saud University, Riyadh 12372, Saudi Arabia*

[a)]*Corresponding author: ckho@sandia.gov*

Abstract. A 1 MW_{th} high-temperature falling particle receiver was constructed and tested at the National Solar Thermal Test Facility at Sandia National Laboratories. The continuously recirculating system included a particle elevator, top and bottom hoppers, and a cavity receiver that comprised a staggered array of porous chevron-shaped mesh structures that slowed the particle flow through the concentrated solar flux. Initial tests were performed with a peak irradiance of ~300 kW/m^2 and a particle mass flow rate of 3.3 kg/s. Peak particle temperatures reached over 700 °C near the center of the receiver, but the particle temperature increase near the sides was lower due to a non-uniform irradiance distribution. At a particle inlet temperature of ~440 °C, the particle temperature increase was 27 °C per meter of drop length, and the thermal efficiency was ~60% for an average irradiance of 110 kW/m^2. At an average irradiance of 211 kW/m^2, the particle temperature increase was 57.1 °C per meter of drop length, and the thermal efficiency was ~65%. Tests with higher irradiances are being performed and are expected to yield greater particle temperature increases and efficiencies.

INTRODUCTION

Falling particle receivers are being investigated to enable higher operating temperatures (>700°C), inexpensive direct storage, and higher receiver efficiencies for concentrating solar power technologies and hydrogen production.[1-16] Unlike conventional receivers that employ fluid flowing through tubular receivers, falling particle receivers use solid particles that are heated directly as they fall through a beam of concentrated sunlight for direct heat absorption. Once heated, the particles may be stored in an insulated tank and used to heat a secondary working fluid for the power cycle on demand. Previous studies have considered alternative particle receiver designs including free-falling,[13] centrifugal,[15, 16] flow in tubes with or without fluidization,[10, 17, 18] multi-pass recirculation,[4, 12] north- or south-facing,[1, 6] and face-down configurations.[19]

In this work, Sandia National Laboratories has led a U.S. Department of Energy SunShot project over the last three years to develop advances in falling particle receiver technology, including optimized receiver geometries, air curtains, discrete porous structures in the particle flow that increase particle residence time and heating, particle characterization and formulations for increased solar absorptance and durability, and new designs for particle storage, heat exchange, and conveyance.[1, 4, 20-30] This work has culminated in a 1 MW_{th} prototype system that has been designed and constructed at Sandia. The objectives of the prototype were to demonstrate a continuously operating particle receiver system that heats the particles to at least 700 °C with 90% efficiency. The remainder of this paper describes the receiver design and on-sun tests of the prototype particle receiver.

RECEIVER DESIGN

Discrete Porous Structures and System Configuration

The receiver design is shown in **FIGURE 1** and consists of a staggered array of stainless-steel chevron-shaped porous mesh structures affixed onto an insulating alumina board (~1.2 m high x 1.2 m wide) inside of a cubical cavity with a ~1 m x 1 m aperture. The particles flow through and over the chevron-shaped mesh structures (similar to a Pachinko board) as they are irradiated by the concentrated solar flux entering through the aperture. [24, 30] The intent of the structures is to slow the particles and increase the residence time within the concentrated flux. After falling through the receiver, the particles are collected in a bottom hopper and funneled into a high temperature Olds particle elevator that lifts the particles inside a rotating casing surrounding a stationary auger. The particles are discharged into the top hopper, where the particles are released into the cavity receiver. The mass flow rate of particles falling into the receiver is controlled by a fixed slot aperture in a discharge plate at the base of the top hopper.[31] The receiver system also includes a water-cooled flux target with a Kendall radiometer that is used to measure and characterize the concentrated irradiance distribution from the heliostat field. The receiver system is instrumented with over 150 thermocouples to record temperatures throughout the system.

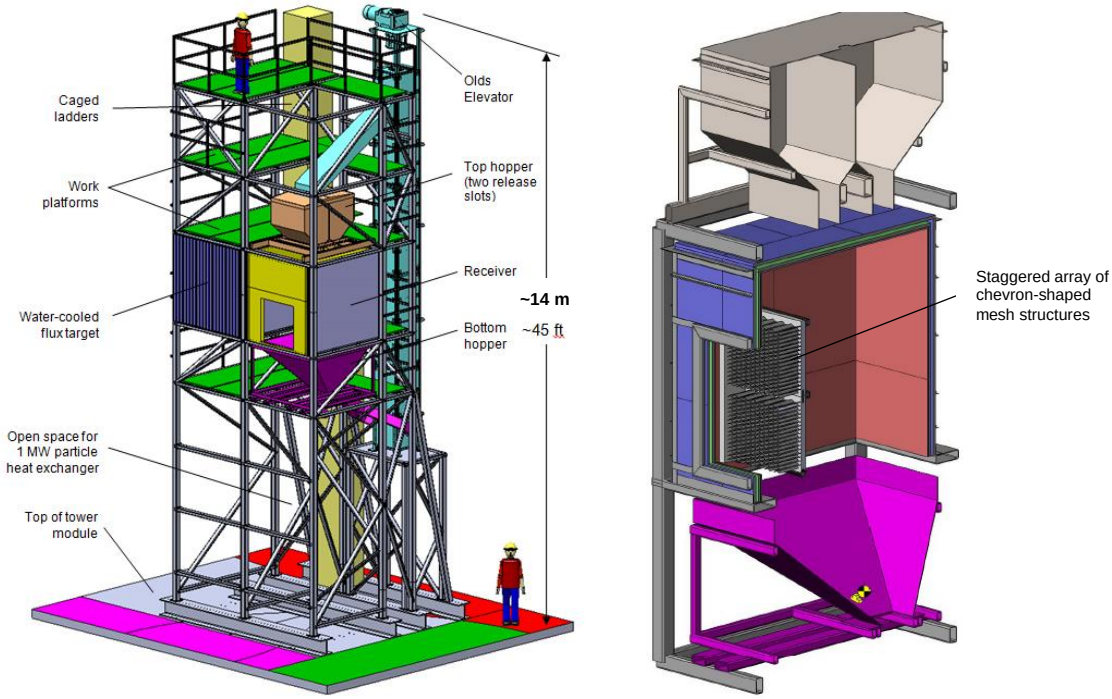

FIGURE 1. Falling particle receiver prototype system (left) and cutaway of the receiver and top and bottom hoppers (right).

Particles and Flow Characterization

The commercially available ceramic particles used in the tests (CARBO Accucast ID50) have excellent optical properties[26, 27] (solar absorptance ~0.9) and are very durable at high temperatures.[20] Physical and thermal properties of the particles used in the tests can be found in Ho et al. (2015).[31] Particle image velocimetry was used to characterize the velocities of the particles flowing over the discrete chevron mesh structures in the receiver. The terminal velocities were measured to be ~0.5 – 0.8 m/s, nearly an order of magnitude lower than the free-fall particle velocity after 1 – 2 m of drop length.[31] The particle mass flow rate through the 1.24 m wide slot (6.35 mm aperture) was measured to be 2.7 kg/s/m or 3.3 kg/s. The depth of the chevrons was ~13 cm, and the slot from the discharge plate was centered over the chevrons. Although most of the chevron surface was covered by flowing particles, the

leading edge (2 – 4 cm) was still visible and exposed to direct irradiance (**FIGURE 2**). This may lead to oxidation and degradation of the mesh structures.

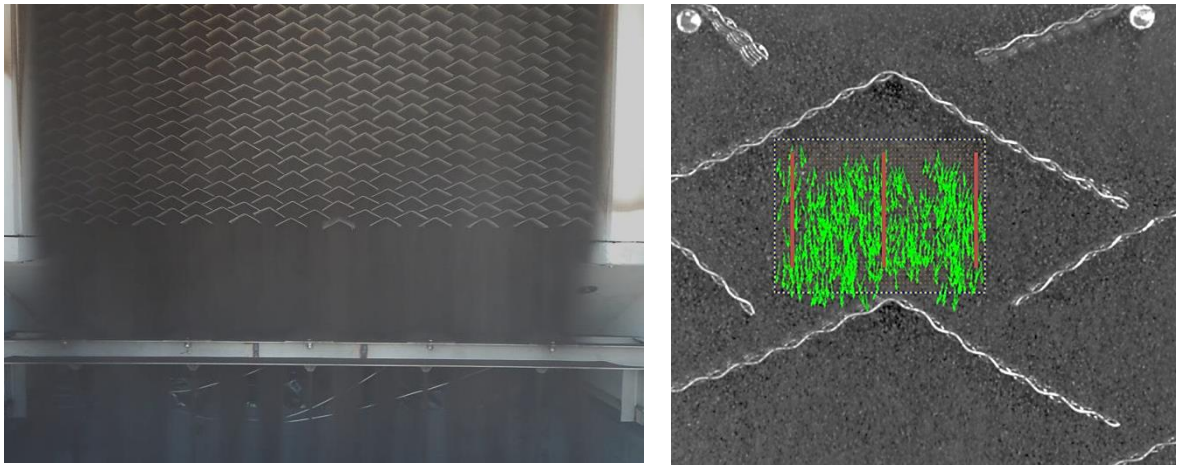

FIGURE 2. Particle flow through the staggered array of chevron-shaped mesh structures in the receiver (left) and PIV calculation on close-up image of particle flow beneath a chevron (right). The green arrows represent particle velocity vectors (predominantly downward) within the interogation region (dashed outline). The three vertical orange lines indicate locations where manual frame-by-frame analysis was performed for verification.

ON-SUN TESTING

Heliostat Field and Tower

The on-sun tests were performed at the National Solar Thermal Test Facility (NSTTF) at Sandia National Laboratories in Albuquerque, New Mexico. The heliostat field consists of over 200 heliostats, each with 37 m^2 of mirrored surface area. The heliostat field can generate 5 – 6 MW of thermal energy to the top of the 61 m (200 ft) tower or any of three test bays. The tower consists of a large elevator module that can lift test articles to the top of the tower. The receiver system was assembled on the elevator module at ground level and then lifted to the top of the NSTTF tower on June 22, 2015. The lift took approximately 7-8 hours, which included reconnection of electrical systems and fire safety equipment. Four cables and jacks were used to hydraulically pull the elevator module and receiver structure (weighing nearly $2x10^5$ kg) to the top of the tower. The receiver system itself weighed about 14,000 kg, including the weight of the particles. **FIGURE 3** shows an image of the on-sun testing.

FIGURE 3. On-sun testing of the particle receiver prototype at the top of the tower. Left: heliostats in standby position. Right: heliostats aimed at receiver.

Irradiance Measurements and Modeling

The irradiance distribution on the receiver was characterized by using photographic images of the combined heliostat beams on the water-cooled flux target adjacent to the receiver. The irradiance on the flux target was photographed and processed using the PHLUX method,[32] and the Kendall radiometer located in the center of the flux target provided an irradiance measurement that was used to scale the pixel values. The ray-tracing tool SolTrace was used to identify heliostat configurations that would produce a desired peak flux and power into the receiver. **FIGURE 4** shows an example of the measured and simulated irradiance distribution on the flux target for a 300-sun peak-flux test. The images are cropped to match the size of the receiver aperture.

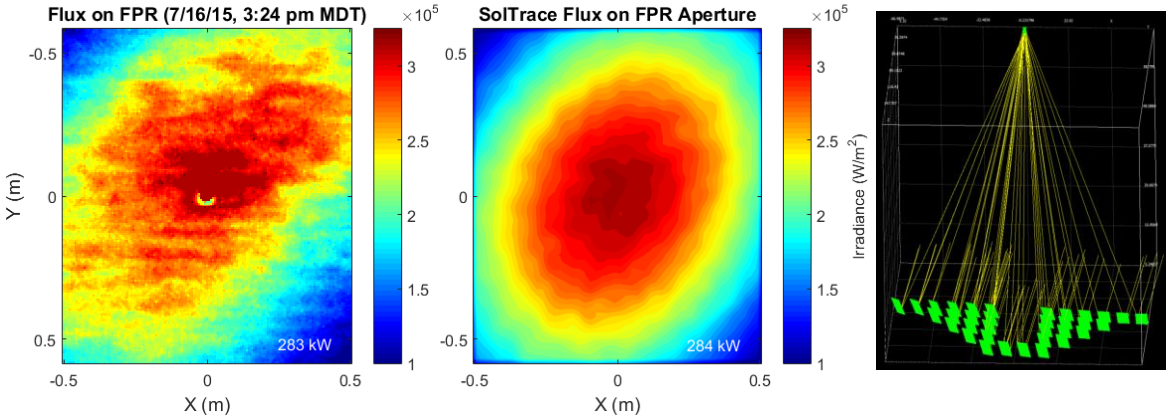

FIGURE 4. Measured (left) and simulated (middle) irradiance distributions on the flux target using SolTrace (right) with a peak flux of ~300 kW/m^2 from 34 heliostats at 15:24 MDT on July 16, 2015.

On July 16, 2015, an on-sun particle flow test was performed with the recirculating receiver. The irradiance distribution was used to determine the power incident on the particles, which was used together with the measured particle temperatures, T (C), particle mass flow rate, $\dot{m}$ (kg/s), and particle specific heat, c_p (J/kg-K), to calculate the thermal efficiency. The particle temperatures entering and leaving the irradiated receiver were recorded using type K thermocouples, which were placed near the outlet of the top hopper and at five locations along the bottom of the receiver beneath the chevron mesh structures (not in the line of sight of the heliostats). The five bottom thermocouples were placed inside stainless steel funnels (10 cm x 10 cm at the top and 1 cm x 1 cm at the bottom) that filled with flowing particles and immersed the thermocouples to ensure an accurate temperature measurement of

the falling particles. The discharge time of the funnels was on the order of ~10 seconds, which was not expected to cause a significant lag in the temperature measurements.

The following protocol was implemented during the tests: (1) turn on the particle elevator to begin particle flow through the system; (2) aim the prescribed heliostats at the water-cooled flux target and measure the irradiance; (3) aim the heliostats at the receiver aperture and heat the particles to a desired (bulk) temperature entering the receiver; (4) at the desired temperature, remove the heliostats and allow the particles to mix and temperatures to stabilize; (5) aim the prescribed heliostats at the receiver aperture to heat the particles and allow temperatures to stabilize for several minutes (there is a 2 – 3 minute recirculation cycle during which time the inlet temperatures are nearly constant after having removed the heliostats); (6) aim heliostats at water-cooled flux target and measure irradiance; (7) repeat steps (3) – (6) as necessary to evaluate particle temperature rise and thermal efficiency at different temperatures.

FIGURE 5 shows a plot of the temperatures during a sequence of stages (steps 4 and 5) when the particle temperature entering the receiver was ~440°C. The particle temperature increase was ~30°C near the edges to ~90°C near the center with average irradiances on the falling particles ranging from ~100 – 200 kW/m^2. **FIGURE 5** also shows the corresponding simulated irradiance distribution on the vertical plane of falling particles (inside the cavity ~0.76 m from the aperture) using the ray-tracing model that was scaled and validated against the measured irradiance on the water-cooled flux target. Because the irradiance distribution was non-uniform, the particle temperature rise was also non-uniform; particles near the center were heated more than the particles near the edges. The five thermocouple readings (TC-BH-005 to TC-BH-009) plotted in **FIGURE 5** (left) correspond to the five zones denoted by the dashed lines on the irradiance plot in **FIGURE 5** (right). Thermocouple TC-BH-005 was located under the far left zone (east), and TC-BH-009 was located under the far right zone (west). The irradiance is not completely symmetric about the center of the receiver because the time of this test was at 15:22 MDT, about two hours after solar noon. The sun was toward the west, and the heliostats on the east side of the field had a better optical efficiency than the heliostats on the west side of the field. Thus, the irradiance on the west side of the receiver was higher.

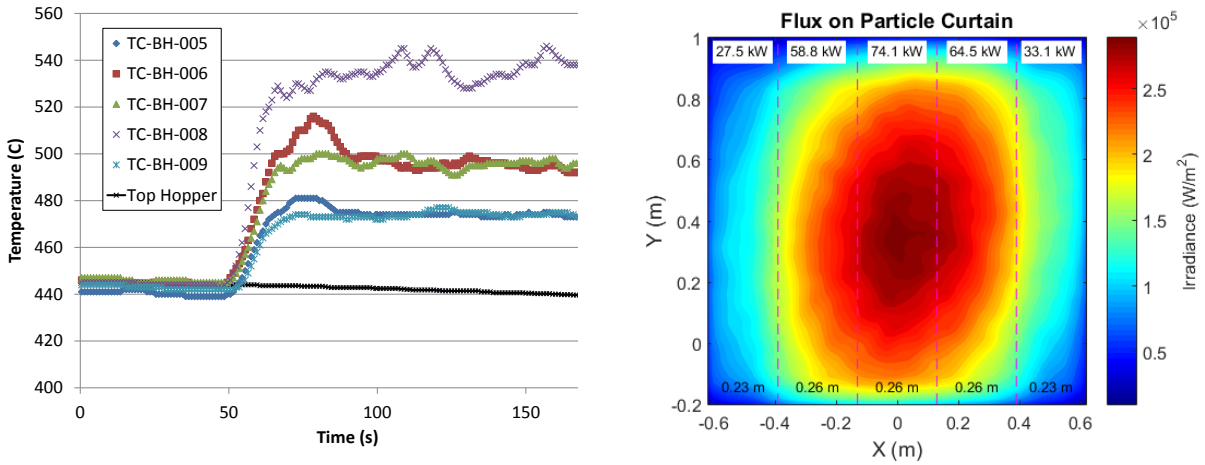

FIGURE 5. Left: measured particle temperatures at the inlet ("Top Hopper") and five outlet locations of the receiver during a test on July 16, 2015 at 15:22 MDT, with a peak flux of ~300 kW/m^2. Right: simulated irradiance on particles; dashed lines denote zones corresponding to the five thermocouple funnels at the bottom of the receiver. TC-BH-005 (east side) is on the left while TC-BH-009 (west side) is on the right.

The thermal efficiency, η_{th}, during the heating stage shown in **FIGURE 5** was calculated as follows:

$$\eta_{th} = \frac{Q_{abs}}{Q_{in}} = \frac{\dot{m}\left(h_{out} - h_{in}\right)}{Q_{in}} = \frac{\dot{m}\int_{T_{in}}^{T_{out}} c_p\left(T\right)dT}{Q_{in}} = \frac{\dot{m}\left[\frac{365}{1.18}\left(T_{out}^{1.18} - T_{in}^{1.18}\right)\right]}{Q_{in}} \quad (1)$$

where Q_{abs} is the power absorbed by the particles (W), Q_{in} is the incident power on the particles, and T_{in} and T_{out} are the inlet and outlet particle temperatures, respectively. In Eq. (1), the following relation[31] derived from measured data for the particle specific heat as a function of temperature (in degrees Celsius) was used:

$$c_p(T) = 365T^{0.18} \tag{2}$$

Since the outlet particle temperatures were measured at five locations beneath the mesh structures in the receiver, the bulk outlet temperature, T_{out}, was determined from the individual temperatures using an energy balance assuming adiabatic mixing as follows:

$$\dot{m}_{out} h_{out} = \sum_i \dot{m}_i h_i \tag{3}$$

The relation, $h=c_pT$, is used together with Eq. (2) and Eq. (3) to yield the following expression for the bulk outlet temperature, where T is expressed in degrees Celsius:

$$T_{out}(C) = \left[\frac{\sum_i \dot{m}_i T_i^{1.18}(C)}{\dot{m}_{out}} \right]^{1/1.18} \tag{4}$$

TABLE 1 shows the resulting data from the 300-sun peak-flux on-sun test, and FIGURE 6 shows a plot of the thermal efficiency as a function of the average irradiance using different irradiated zones shown in FIGURE 5. The inner three zones received the highest flux, while the outer two zones received the lowest flux. The measured efficiency ranged from 60% for an average irradiance of 110 kW/m^2 to 65% for an average irradiance of 211 kW/m^2. As expected, the thermal efficiency was greater when the irradiance was higher under otherwise similar conditions. The propagated uncertainty accounted for uncertainty in measurements of the particle mass flow rate, temperatures, and irradiance. Future tests will include higher peak fluxes and higher particle (bulk) temperatures. It should be noted that outlet particle temperatures of over 700 °C have been reached in recent tests with peak fluxes of ~700 kW/m^2. At these higher irradiances, we expect to achieve greater than 80% thermal efficiency.

TABLE 1. Results from on-sun test with peak irradiance of ~300 kW/m^2 (15:22 MDT, July 16, 2015).

Location	Average Irradiance (kW/m^2)	Average Particle ΔT per drop length (°C/m)	Average Particle Temperature (°C)	Specific Heat (J/kg-K)	Mass Flow Rate (kg/s)	Power absorbed by particles (kW)	Incident Power (kW)	Thermal Efficiency	Propagated ± Error in Efficiency
Outer two zones	110	27.4	457	1100	1.0	44.4	60.6	0.596	0.123
All zones	173	46.1	469	1100	2.7	203	258	0.639	0.132
Inner three zones	211	57.1	475	1110	1.7	158	197	0.652	0.135

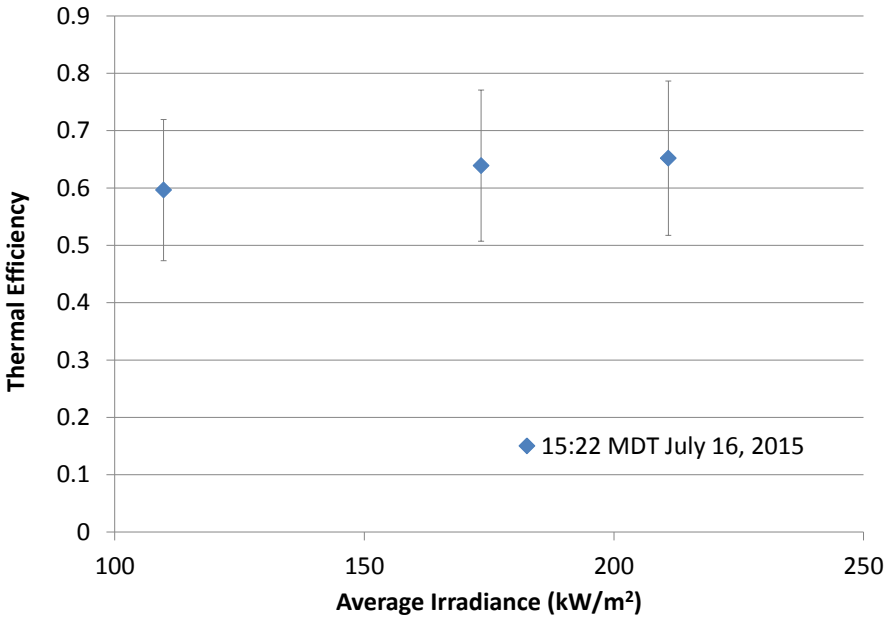

FIGURE 6. Thermal efficiency as a function of average irradiance on particles.

CONCLUSIONS

A high-temperature (>700 °C) 1 MW_{th} continuously recirculating falling particle receiver has been constructed and tested at the National Solar Thermal Test Facility at Sandia National Laboratories in Albuquerque, New Mexico. Commercially available ceramic particles with high solar absorptance and good durability at high temperatures were used. The receiver design comprised staggered chevron mesh structures that slowed the particles and increased their residence time within the concentrated solar flux. Concentrated sunlight entered the cavity receiver through a ~1 m x 1 m aperture. The particles were lifted to the top of the system using an Olds elevator with a rotating casing around a stationary auger. The particles were then discharged into the receiver from a top hopper with a fixed slot aperture that controlled the mass flow rate at ~3.3 kg/s. After falling through the receiver, the particles were collected in a bottom hopper and funneled to the base of the elevator where the particles were then recirculated back to the top. A water-cooled flux target was used to characterize the irradiance distribution.

On-sun testing was performed with a peak flux of ~300 suns, and the following conclusions were made:

- The system was successfully operated with continuous recirculation of particles, and peak particle temperatures reached over 700 °C
- The non-uniform irradiance caused non-uniform heating of particles; the particles near the center of the receiver were heated the most while particles near the edges were heated the least
- At a particle inlet temperature of ~440 °C, the average particle temperature rise per unit drop length was ~27 °C/m at an average particle irradiance of 110 kW/m^2. At an average irradiance of 211 kW/m^2, the particle temperature rise per unit drop length was ~57 °C/m.
- The receiver thermal efficiency was positively correlated to the amount of irradiance on the particles; the thermal efficiency at particle inlet temperatures of ~440 °C ranged from ~60% to 65% for average particle irradiances ranging from 110 and 211 kW/m^2

ACKNOWLEDGMENTS

The authors thank JJ Kelton, Daniel Ray, Kye Chisman, Doug Robb, Benson Tso, Bill Kolb, Ryan Anderson, Ron Briggs, and Steve Hinken for their contributions on the receiver assembly and testing. Sandia National Laboratories is a multi-program laboratory managed and operated by Sandia Corporation, a wholly owned subsidiary of Lockheed Martin Corporation, for the U.S. Department of Energy's National Nuclear Security Administration under contract DE-AC04-94AL85000.

REFERENCES

1. J. M. Christian and C. K. Ho, in *SolarPACES 2013* (Las Vegas, NV, 2013).
2. P. K. Falcone, J. E. Noring and J. M. Hruby, 1985.
3. B. Gobereit, L. Amsbeck, R. Buck, R. Pitz-Paal and H. Müller-Steinhagen, in *SolarPACES 2012* (Marrakech, Morrocco, 2012).
4. C. Ho, J. Christian, D. Gill, A. Moya, S. Jeter, S. Abdel-Khalik, D. Sadowski, N. Siegel, H. Al-Ansary, L. Amsbeck, B. Gobereit and R. Buck, Proceedings of the Solarpaces 2013 International Conference **49** (Energy Procedia), 398-407 (2014).
5. J. M. Hruby and B. R. Steele, Chem Eng Prog **82** (2), 44-47 (1986).
6. S. S. S. Khalsa, J. M. Christian, G. J. Kolb, M. Röger, L. Amsbeck, C. K. Ho, N. P. Siegel and A. C. Moya, (ASME International Conference on Energy Sustainability, Washington, DC, USA, 2011).
7. S. S. S. Khalsa and C. K. Ho, J Sol Energ-T Asme **133** (3) (2011).
8. K. Kim, S. F. Moujaes and G. J. Kolb, Sol Energy **84** (2), 263-270 (2010).
9. G. J. Kolb, R. B. Diver and N. Siegel, J Sol Energ-T Asme **129** (2), 179-183 (2007).
10. Z. W. Ma, G. Glatzmaier and M. Mehos, J Sol Energ-T Asme **136** (3) (2014).
11. M. J. Rightley, L. K. Matthews and G. P. Mulholland, Sol Energy **48** (6), 363-374 (1992).
12. M. Röger, L. Amsbeck, B. Gobereit and R. Buck, Journal of Solar Energy Engineering (2011).
13. N. P. Siegel, C. K. Ho, S. S. Khalsa and G. J. Kolb, J Sol Energ-T Asme **132** (2) (2010).
14. T. D. Tan and Y. T. Chen, Renew Sust Energ Rev **14** (1), 265-276 (2010).
15. W. Wu, D. Trebing, L. Amsbeck, R. Buck and R. Pitz-Paal, J Sol Energ-T Asme **137** (4) (2015).
16. W. Wu, R. Uhlig, R. Buck and R. Pitz-Paal, Numer Heat Tr a-Appl **68** (2), 133-149 (2015).
17. G. Flamant, D. Gauthier, H. Benoit, J. L. Sans, B. Boissiere, R. Ansart and M. Hemati, Proceedings of the Solarpaces 2013 International Conference **49**, 617-626 (2014).
18. G. Flamant, D. Gauthier, H. Benoit, J. L. Sans, R. Garcia, B. Boissiere, R. Ansart and M. Hemati, Chem Eng Sci **102**, 567-576 (2013).
19. M. Röger, L. Amsbeck, B. Gobereit and R. Buck, in *J Sol Energ-T Asme* (2011), Vol. 133.
20. Al-Ansary H. et al., in *SolarPACES 2013* (Las Vegas, NV, 2013).
21. J. M. Christian and C. K. Ho, Proceedings of the Solarpaces 2014 International Conference (Energy Procedia) (2014).
22. C. K. Ho and J. M. Christian, in *Proceedings of ASME 2013 7th International Conference on Energy Sustainability* (Minneapolis, MN, 2013).
23. C. K. Ho, J. M. Christian, A. C. Moya, J. Taylor, D. Ray and J. Kelton, in *Proceedings of ASME 2014 8th International Conference on Energy Sustainability* (Minneapolis, MN, 2014).
24. A. W. Khayyat, R. C. Knott, C. L. Nguyen, M. C. Golob, S. I. Abdel-Khalik, S. M. Jeter and H. A. Al-Ansary, in *Proceedings of the ASME 2015 Power and Energy Conversion Conference* (San Diego, CA, 2015).
25. C. Nguyen, D. Sadowski, A. Alrished, H. Al-Ansary, S. Jeter and S. Abdel-Khalik, Proceedings of the Solarpaces 2013 International Conference **49**, 637-646 (2014).
26. N. Siegel, M. Gross, C. Ho, T. Phan and J. Yuan, Proceedings of the Solarpaces 2013 International Conference **49** (Energy Procedia), 1015-1023 (2014).
27. N. P. Siegel, M. D. Gross and R. Coury, ASME J. Solar Energy Eng. **137** (4), 041003-041003-041007 (2015).
28. R. Knott, D. L. Sadowski, S. M. Jeter, S. I. Abdel-Khalik, H. A. Al-Ansary and A. El-Leathy, in *Proceedings of the ASME 2014 8th International Conference on Energy Sustainability* (Boston, MA, 2014).
29. R. Knott, D. L. Sadowski, S. M. Jeter, S. I. Abdel-Khalik, H. A. Al-Ansary and A. El-Leathy, in *Proceedings of the ASME 2014 8th International Conference on Energy Sustainability* (Boston, MA, 2014).
30. T. Lee, S. Lim, S. Shin, D. L. Sadowski, S. I. Abdel-Khalik, S. M. Jeter and H. Al-Ansary, Sol Energy **113**, 14-24 (2015).
31. C. K. Ho, J. M. Christian, D. Romano, J. Yellowhair and N. Siegel, in *Proceedings of the ASME 2015 Power and Energy Conversion Conference* (San Diego, CA, 2015).
32. C. K. Ho and S. S. Khalsa, J Sol Energ-T Asme **134** (4) (2012).